applied sciences

MDPI

Article

Analysis of Optical Integration between Si_3N_4 Waveguide and a Ge-Based Optical Modulator Using a Lateral Amorphous GeSi Taper at the Telecommunication Wavelength of 1.55 μm

Worawat Traiwattanapong [1], Kazumi Wada [2,3] and Papichaya Chaisakul [1,*]

1 Department of Physics, Faculty of Science, Kasetsart University, Bangkok 10900, Thailand; worawat.tra@ku.th
2 Department of Materials Engineering, the University of Tokyo, Bunkyo 113-8656, Japan; kwada@mit.edu
3 Department of Materials Science and Engineering, Massachusetts Institute of Technology, Cambridge, MA 02139, USA
* Correspondence: fscipac@ku.ac.th

Received: 15 August 2019; Accepted: 10 September 2019; Published: 13 September 2019

check for updates

Abstract: We report on the theoretical investigation of using an amorphous $Ge_{0.83}Si_{0.17}$ lateral taper to enable a low-loss small-footprint optical coupling between a Si_3N_4 waveguide and a low-voltage Ge-based Franz–Keldysh optical modulator on a bulk Si substrate using 3D Finite-Difference Time-Domain (3D-FDTD) simulation at the optical wavelength of 1550 nm. Despite a large refractive index and optical mode size mismatch between Si_3N_4 and the Ge-based modulator, the coupling structure rendered a good coupling performance within fabrication tolerance of advanced complementary metal-oxide semiconductor (CMOS) processes. For integrated optical modulator performance, the Si_3N_4-waveguide-integrated Ge-based on Si optical modulators could simultaneously provide workable values of extinction ratio (ER) and insertion loss (IL) for optical interconnect applications with a compact footprint.

Keywords: germanium; silicon nitride; optical interconnect; Franz–Keldysh effect

1. Introduction

Photonic–electronic convergence on silicon (Si) has the strong potential to provide high-volume, low-cost, and energy-efficient solutions to the increasingly-high bandwidth demands for data center interconnects and long-haul telecommunication networks [1–4]. In this regard, Ge-on-Si photonic devices are promisingly being developed in waveguide configurations for optical modulation, detection, and emission around the C-band telecommunication wavelength of 1.55 μm [5]. Accordingly, efficient integration between Ge-based photonic devices and crystalline Si on insulator (SOI) waveguides are the subject of intense research in order to enable on-chip integration between various photonic devices on SOI substrates. Ge-based optical modulators and photodetectors integrated with SOI waveguide were developed with very impressive high-speed performance at 1.55 μm [6–14], using electro-absorption based on the Franz–Keldysh effect (FKE), which is intrinsically fast [15]. Nevertheless, to integrate photonics with complementary metal-oxide semiconductor (CMOS) electronics and take full advantage of large-scale manufacturing, it is also of importance to have the capability to monolithically develop photonic circuitry on bulk Si substrate [16–18], which could be a significant challenge for SOI-based devices. Moreover, in order to further accommodate a rapid increase in data traffic, the adoption of wavelength multiplexing is considered critical. In these regards, Si_3N_4 waveguide could be regarded as a promising alternative suitable for wavelength division multiplexing implementation in photonic integrated circuits on bulk Si substrate [19–23]. Due to the relatively-low thermo-optics coefficient of Si_3N_4 and a moderate refractive index contrast between Si_3N_4 and SiO_2, Si_3N_4 was proposed to be advantageous for wavelength multiplexing in terms of polarization independence, phase error due to fabrication imperfections, temperature stability, and wideband operation for telecommunications applications [23–25]. Additionally, a Si_3N_4 refractive index ~2 is sufficiently high to realize compact photonic circuits with SiO_2 cladding (n ~ 1.45) [20,23]. Moreover, silicon nitride-based waveguides can possibly be deposited directly onto bulk Si substrate at a relatively low temperature [23,26,27]. Nevertheless, comparing to SOI waveguides, efficient optical coupling between Si_3N_4 waveguide and Ge-on-Si photonic components could be considered significantly more challenging due to an even larger refractive index difference between Si_3N_4 and Ge.

In this paper, we propose and present theoretical analysis on the use of a compact amorphous GeSi lateral taper (15 μm in length) to facilitate the optical coupling between a Si_3N_4 waveguide (refractive index of ~2), and a low-voltage Ge-based FKE optical modulator (refractive index of ~4.3) using 3D Finite-Difference Time-Domain (3D-FDTD) simulation (Lumerical Inc. Vancouver, BC, Canada) at the optical wavelength of 1.55 μm. As there was no need for a crystalline layer for its deposition, the amorphous material was grown on SiO_2 layers, providing design flexibility to obtain the most suitable configuration of optimized optical coupling; moreover, it was also possible to develop the structure on bulk Si substrate. Coupling structure in a lateral direction was used in order to be preferable for quasi-transverse-electric (quasi-TE) polarization, which was typically employed for Ge-based Franz–Keldysh optical modulators in waveguide configuration [6–9]. Additionally, it should be noted that there were mainly two approaches to obtain FKE at 1.55 μm from Ge, which were either by the use of Ge-rich GeSi such as $Ge_{0.9925}Si_{0.0075}$ (adding a very small amount of Si) [28], or by the application of compressive strain on pure Ge [29]. The proposed coupling structure should render a very similar performance in both cases as the refractive index of the Ge-rich GeSi and Ge are almost identical. We found that the proposed coupling structure could be employed to enable Si_3N_4 waveguide integrated Ge-based optical modulator with a viable performance in term of extinction ratio and insertion loss with a compact footprint. The analysis of performance variation with respect to fabrication variation is also presented here with promising prospects. Also, it should be noted that although good optical coupling performance was demonstrated experimentally [30] and theoretically [31] from Ge-on-Si photodetector integrated directly with a silicon nitride waveguide, there is no need to maintain the fundamental mode inside and at the output of a photodetector, as required in the case of an optical modulator; therefore, for photodetector Ge can be made relatively large to accommodate optical coupling with silicon nitride. In addition, for Ref. 24 the integration of the Si_3N_4 waveguide with Ge-on-Si photodetector was performed via SOI waveguide; thus, the SOI wafer was employed.

2. Optical Coupling Structures

We focused on the optical coupling between the fundamental optical mode of the 1 μm high and 1 μm wide Si_3N_4 waveguide (Figure 1a) and the fundamental mode of the 200 nm high and 590 nm wide Ge-based FKE optical modulator (Figure 1c). The optical mode from Si_3N_4 had an effective index of ~1.79, which was significantly smaller than the effective index of ~3.55 obtained from the Ge-based on Si structure. Moreover, the optical mode size of the former was much larger than that of the latter, which was well-confined in the Ge-based material due to its larger refractive index than that of the top and bottom Si (n ~ 3.45). It should be noted that decreasing the Si_3N_4 dimension lowered its effective index and also eventually made the optical mode size larger as the optical power spread out of the Si_3N_4 core, which was not beneficial for direct optical coupling with the compact Ge-based FKE optical modulator. Modulators are typically required to have a relatively smaller dimensions in order to allow high electric field at low bias voltage, which is critical for low-voltage operation. In this paper, the lateral amorphous GeSi taper was optimized for optical coupling with the 200 nm high and 590 nm wide Ge-based FKE optical modulator; this coupling structure should be able to be adapted to other compact Ge-based devices with comparable dimensions with corresponding adjustments in taper width, height, and length. Additionally, it should be noted that although a butt coupling structure was proposed at the telecommunication wavelength of 1.31 µm for optical integration between a Si_3N_4 waveguide and Ge/SiGe multiple quantum wells (MQWs) on Ge-rich SiGe buffer devices [32], their optical mode areas were relatively comparable, which was not the case for the Ge-on-Si device, in which a large index difference between Ge-based modulator region and Si resulted in a highly confined and much smaller optical mode in the Ge-based region, as shown Figure 1c. Regarding the amorphous taper's dimensions, its length and height were 15 µm and 200 nm, respectively, while the width at the beginning and at the end of the taper were 30 nm and 290 nm, respectively. The aspect ratio of ~6.7 (200/30) at the beginning of the taper could be considered critical; nevertheless, it was within the capability of the advanced CMOS deep etching process. Regarding the possibility of practical fabrication for 1 µm thick SiN, it was proposed by Ref. 23 that physical vapor deposition (PVD) had the potential to achieve a low-loss SiN material with maximum thickness beyond that normally obtainable with chemical vapor deposition (CVD) due to its lower built-in stress. Performance variation with respect to the change in taper tip width is discussed in the next section. The top cladding employed in simulation was SiO_2; therefore, the etching was stopped on the SiO_2 surface used to support the amorphous taper. The SiO_2 top cladding is not included in Figure 1d to allow a clear demonstration of the entire integrated devices. As in Figure 1e for the top view of optical propagation, the optical mode was transferred from the 1 µm high and 1 µm wide Si_3N_4 waveguide to the 200 nm high and 590 nm wide Ge-based modulator region via the amorphous $Ge_{0.83}Si_{0.17}$ taper (Figure 1b). For the Ge-based FKE p-i-n structure, the top Si n-layer and the bottom Si p-layer were 200 nm and 400 nm high, respectively. The bottom Si p-layer had a 200 nm etching depth to accommodate the bottom contact metallization. Regarding the optical parameters employed in simulation, the absorption coefficient data of the Ge-based material were as previously reported from $Ge_{0.9925}Si_{0.0075}$ FKE modulator by Liu et al. [28] at the optical wavelength of 1.55 µm. We focused on the absorption change due to the Franz–Keldysh effect between the electric field of 10 kV/cm (α ~ 150 cm^{-1}) and 95 kV/cm (α ~ 650 cm^{-1}) for 200 nm thick $Ge_{0.9925}Si_{0.0075}$ layer, in order to be compatible with a ≤2 V drivable voltage of CMOS [2,9,33]. The free carrier absorption in the p- and n-layers was calculated using the Drude model, with a doping concentration of ~1×10^{18} cm^{-3}. For the amorphous taper, the real part (n ~ 4.08) and the imaginary part (n ~ 0.002468, α ~ 200 cm^{-1}) of amorphous $Ge_{0.83}Si_{0.17}$ were experimentally reported by Hernández-Montero et al. [34] at the optical wavelength of 1.55 µm; therefore, optical absorption due to amorphous material was properly taken into account in this simulation. Variation of Ge concentration in the amorphous material resulted in refractive index variation, which is further verified in the following section.

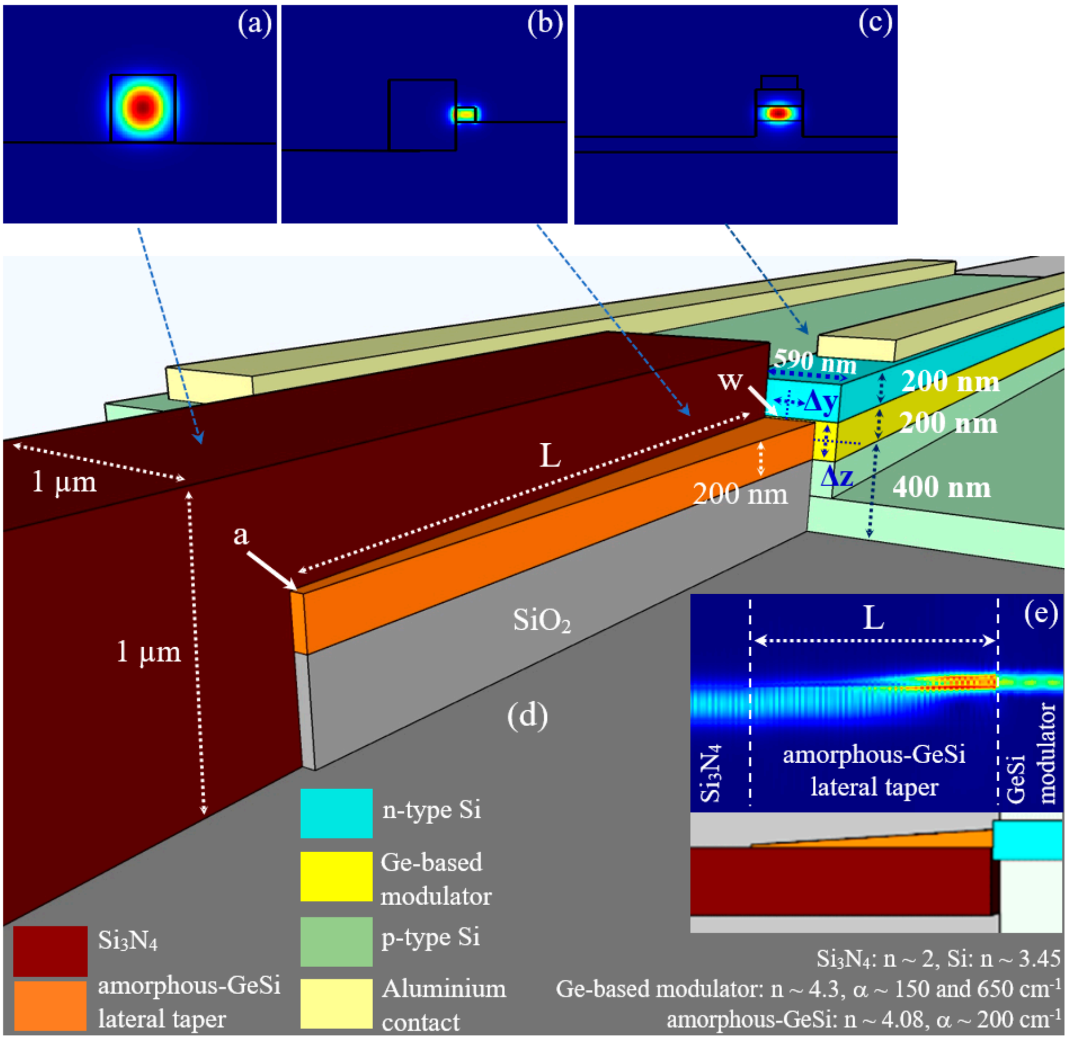

Figure 1. The fundamental optical mode of (**a**) 1 μm high and 1 μm wide Si_3N_4 waveguide, (**b**) amorphous-GeSi lateral taper, and (**c**) 200 nm high and 590 nm wide Ge-based Franz–Keldysh effect (FKE) optical modulator. (**d**) Schematic view of the proposed coupling structure. (**e**) Top view of optical propagation from the Si_3N_4 waveguide via amorphous $Ge_{0.83}Si_{0.17}$ taper to the Ge-based FKE optical modulator.

3. Coupling Performance and Integrated Optical Modulator

Figure 2 reports on the optical coupling performance based on different parameters of the proposed amorphous GeSi taper. To verify the potential of achieving a relatively homogenous performance with a modern, large-scale manufacturing of the Si wafer, we studied the variation in optical coupling based on taper tip width (Figure 2a), taper end width (Figure 2b), taper length (Figure 2c), amorphous $Ge_{0.83}Si_{0.17}$ refractive index (Figure 2d), and the relative positions between the taper and the Ge-based FKE optical modulator (Figure 2e,f). The coupling loss between the 1 μm wide, 1 μm high Si_3N_4 waveguide and the 200 nm thick, 590 nm wide Ge-based FKE layer could be as low as 1.2 dB. As in Figure 2a, a relatively-consistent coupling loss of 1.2 dB was maintained as long as the taper tip width did not become larger than 50 nm. Optical coupling loss became slightly better as the taper tip width became smaller than 10 nm, which could be attributed to a better optical mode matching with the Si_3N_4 waveguide at the tip of the taper. We selected the taper tip width of 30 nm, which gave a good compromise between optical coupling performance and fabrication tolerance. For the taper end width, as in Figure 2b, 1.2 dB coupling loss was sustained for the width variation of ±≤10 nm, which was comparable with that of taper tip width. For the length of the taper, optimized coupling performance of 1.2 dB was achieved with a 15 μm long taper, and only significant fabrication variation of larger than ±0.5 μm (500 nm) began to affect the optimized coupling loss value, as shown Figure 2c. As a variation in the refractive index of deposited amorphous GeSi was reasonably expected, Figure 2d investigates its effect on the coupling performance. It would have taken a refractive index variation of more than ±0.5% to cause a noticeable increase in coupling loss, which was within the capability of modern deposition tools. For the variation in the relative position between the amorphous $Ge_{0.83}Si_{0.17}$ taper and the Ge-based FKE optical modulator, as reported in Figure 2e,f, the optimized coupling performance was maintained as long as the misalignment of vertical and horizontal positions were within ±10 nm. As a result, it was certain that the proposed taper structure could be realized with homogenous performance with respect to the capability of advanced microelectronic process technology [35–37]. It should be noted that we focused the conversation on the ability to maintain optimized optical coupling, as each dB increase in optical loss necessitated a correspondingly higher laser optical power; therefore, the ability to maintain low optical loss was crucial for low-power optical interconnection.

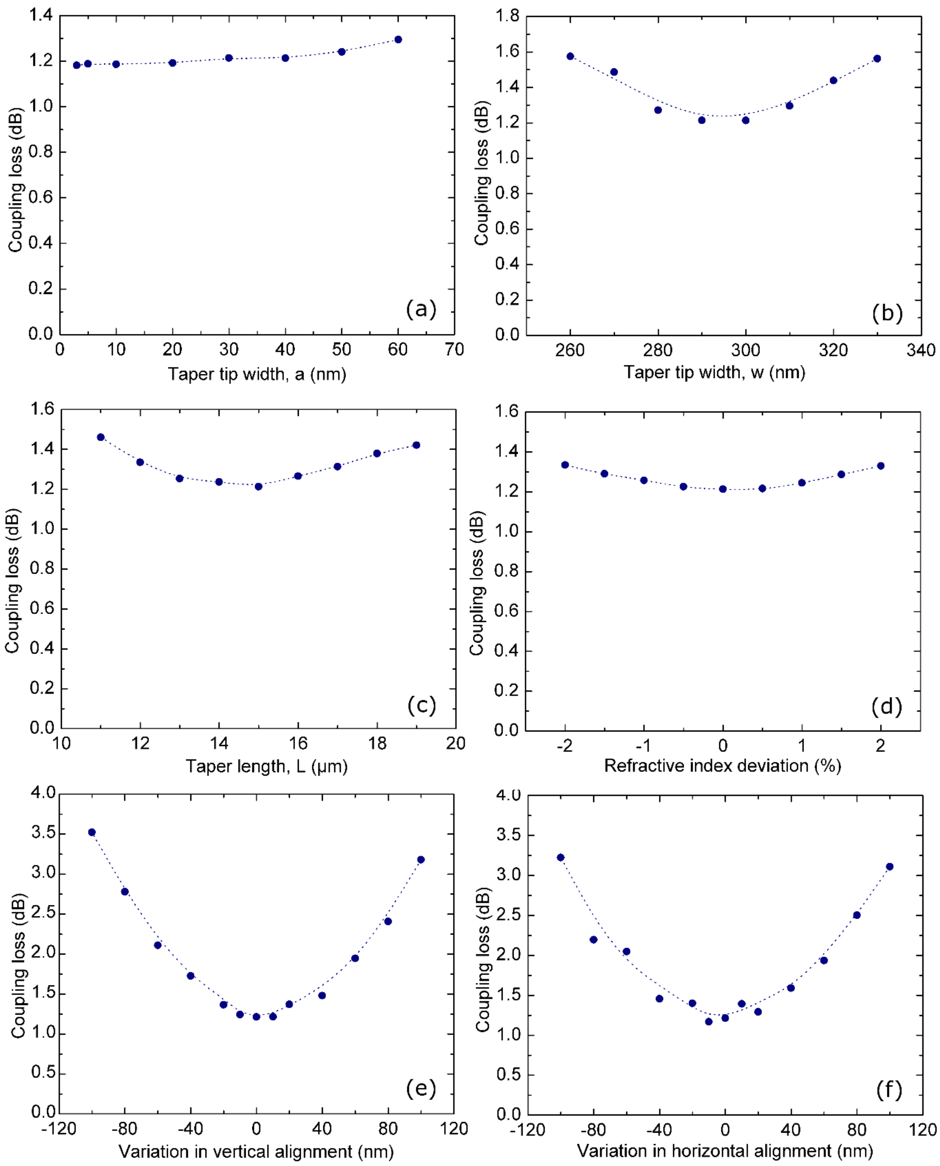

Figure 2. Optical coupling variation with respect to (**a**) taper tip width, (**b**) taper end width, (**c**) taper length, (**d**) amorphous $Ge_{0.83}Si_{0.17}$ refractive index, and the relative (**e**) vertical and (**f**) horizontal positions between the taper and the Ge-based FKE optical modulator.

Figure 3 reports integrated optical modulation performance of the proposed structure consisting of the Si_3N_4 input waveguide, the amorphous $Ge_{0.83}Si_{0.17}$ taper, the Ge-based on Si optical modulator, the amorphous $Ge_{0.83}Si_{0.17}$ taper, and the Si_3N_4 output waveguide using 3D-FDTD simulation (Lumerical Inc. Vancouver, BC, Canada) for the fundamental transverse-electric (TE) mode at the optical wavelength of 1550 nm. As shown in Figure 3a, the optical mode propagated from the input Si_3N_4 waveguide to the output Si_3N_4 waveguide effectively. Figure 3b shows that both the extinction ratio (ER), $10\log10(I_{Out,On}/I_{Out,Off})$, and the insertion loss (IL), $10\log10(I_{In}/I_{Out})$, increased as the length of the Ge-based device increased. Interestingly, the structure obtained an integrated performance of ~5 dB ER simultaneously with ~5 dB on-state IL with the modulator length of 15 µm. This reported IL included the coupling loss between the Si_3N_4 input (respectively output) waveguide and the Ge-based on Si device, the optical absorption due to amorphous taper, and the optical absorption due to the Ge-based on Si structure in high transmission mode. The integrated performance of the 5 dB ER and the 5 dB IL were comparable to the state-of-the-art Ge-based FKE optical modulators integrated with an SOI waveguide [7–9]. It should be noted that a higher ER/IL ratio could have been achieved with longer device. For instance, ~6.7 dB ER and ~5.8 dB IL could have been obtained with a 20 µm long device. Nevertheless, higher optical loss due to Ge indirect-gap absorption makes this undesirable for low-power applications. Figure 3c,d report the ER and IL values with respect to the variation in the relative vertical positions between the amorphous taper and the GeSi optical modulator for the 15 µm long and 20 µm long Ge-on-Si optical modulator, respectively. While the ER values were relatively robust against fabrication misalignment in both cases, the IL values tolerated fabrication misalignment of $\pm \leq 20$ nm in order to maintain the optimized values of ER and IL simultaneously.

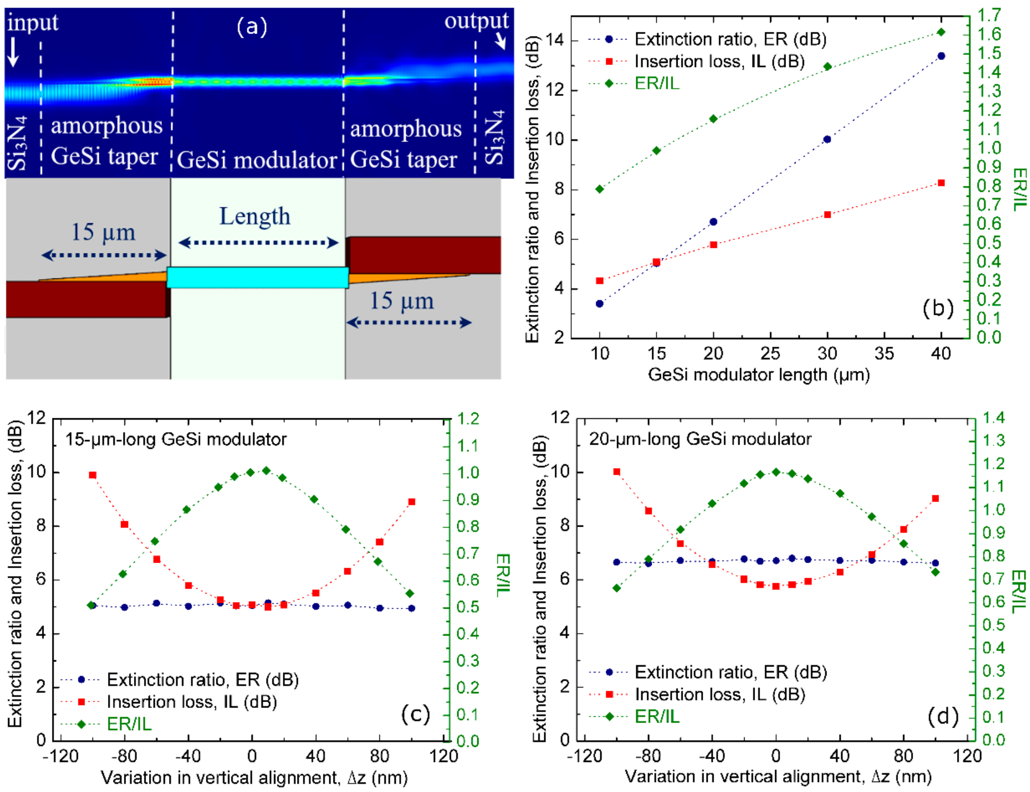

Figure 3. (**a**) Optical propagation from Si_3N_4 input waveguide, amorphous $Ge_{0.83}Si_{0.17}$ taper, Ge-based FKE optical modulator, and amorphous $Ge_{0.83}Si_{0.17}$ taper to the Si_3N_4 output waveguide. (**b**) Extinction ratio (ER) and insertion loss (IL) at different length values of the optical modulator. ER and IL with respect to the variation in the relative vertical positions between the amorphous taper and the Ge-based on Si optical modulator for (**c**) 15 µm long and (**d**) 20 µm long optical modulators, respectively.

4. Conclusions

In conclusion, we theoretically investigated the use of amorphous $Ge_{0.83}Si_{0.17}$ to enable a low-loss small-footprint optical coupling between a Si_3N_4 waveguide and a low-voltage Ge-based on Si optical modulator on bulk Si substrate. Despite a large refractive index and mode-size mismatch between Si_3N_4 and the Ge-based modulator, the results showed that the coupling structure rendered a good coupling performance with a viable fabrication tolerance for large-scale advanced CMOS manufacturing on a Si wafer. From the 3D-FDTD simulation, the Si_3N_4-waveguide-integrated Ge-based optical modulators simultaneously provided usable values of ER and IL, which were comparable to the reported performance obtained from the SOI-integrated Ge-based optical modulator devices [3], for optical interconnect applications at the optical wavelength of 1.55 μm with a compact footprint. Moreover, it should also be noted that the proposed coupling structure could be applicable with different Ge concentrations in amorphous GeSi for a wider range of operating wavelengths regarding optical integration between different Ge-based active devices and silicon nitride waveguides, which will be the subject of future investigation.

Author Contributions: Conceptualization, K.W. and P.C.; data curation, W.T.; formal analysis, W.T. and P.C.; investigation, W.T.; supervision, K.W. and P.C.; writing—original draft, P.C.; writing—review and editing, K.W.

Funding: This research was funded by Kasetsart University Research and Development Institute (KURDI), and Thailand Research Fund and the Office of the Higher Education Commission (MRG6180286).

Acknowledgments: W.T. acknowledges supports from the Institute for the Promotion of Teaching Science and Technology.

Conflicts of Interest: The authors declare no conflict of interest.

References

1. Miller, D.A.B. Device requirements for optical interconnects to silicon chips. *Proc. IEEE* **2009**, *97*, 1166–1185. [CrossRef]
2. Thomson, D.; Zilkie, A.; Bowers, J.E.; Komljenovic, T.; Reed, G.T.; Vivien, L.; Marris-Morini, D.; Cassan, E.; Virot, L.; Fédéli, J.-M.; et al. Roadmap on silicon photonics. *J. Opt.* **2016**, *18*, 073003. [CrossRef]
3. Wang, X.; Liu, J. Emerging technologies in Si active photonics. *J. Semicond.* **2018**, *39*, 061001. [CrossRef]
4. Zhou, Z.; Chen, R.; Li, X.; Li, T. Development trends in silicon photonics for data centers. *Opt. Fiber Technol.* **2018**, *44*, 13–23. [CrossRef]
5. Wada, K.; Kimerling, L.C. *Photonics and Electronics with Germanium*; Wiley-VCH Verlag GmbH & Co. KGaA: Weinheim, Germany, 2015.
6. Liu, J.F.; Beals, M.; Pomerene, A.; Bernardis, S.; Sun, R.; Cheng, J.; Kimerling, L.C.; Michel, J. Waveguide-integrated, ultralow-energy GeSi electro-absorption modulators. *Nat. Photonics* **2008**, *2*, 433–437. [CrossRef]
7. Feng, D.; Liao, S.; Liang, H.; Fong, J.; Bijlani, B.; Shafiiha, R.; Luff, B.J.; Luo, Y.; Cunningham, J.; Krishnamoorthy, A.V.; et al. High speed GeSi electro-absorption modulator at 1550 nm wavelength on SOI waveguide. *Opt. Express* **2012**, *20*, 22224–22232. [CrossRef] [PubMed]
8. Srinivasan, S.A.; Pantouvaki, M.; Gupta, S.; Chen, H.T.; Verheyen, P.; Lepage, G.; Roelkens, G.; Saraswat, K.; van Thourhout, D.; Absil, P.; et al. 56 Gb/s germanium waveguide electro-absorption modulator. *J. Lightwave Technol.* **2016**, *34*, 419–424. [CrossRef]
9. Krishnamoorthy, A.V.; Zheng, X.; Feng, D.; Lexau, J.; Buckwalter, J.F.; Thacker, H.D.; Liu, F.; Luo, Y.; Chang, E.; Amberg, P.; et al. A low-power, high-speed, 9-channel germanium-silicon electro-absorption modulator array integrated with digital CMOS driver and wavelength multiplexer. *Opt. Express* **2014**, *22*, 12289–12295. [CrossRef]
10. Michel, J.; Liu, J.F.; Kimerling, L.C. High-performance Ge-on-Si photodetectors. *Nat. Photonics* **2010**, *4*, 527–534. [CrossRef]
11. Vivien, L.; Polzer, A.; Marris-Morini, D.; Osmond, J.; Hartmann, J.M.; Crozat, P.; Cassan, E.; Kopp, C.; Zimmermann, H.; Fédéli, J.M. Zero-bias 40 Gbit/s germanium waveguide photodetector on silicon. *Opt. Express* **2012**, *20*, 1096–1101. [CrossRef]

12. Zhang, Y.; Yang, S.; Yang, Y.; Gould, M.; Ophir, N.; Lim, A.E.-J.; Lo, G.-Q.; Magill, P.; Bergman, K.; Baehr-Jones, T.; et al. A high-responsivity photodetector absent metal-germanium direct contact. *Opt. Express* **2014**, *22*, 11367–11375. [CrossRef] [PubMed]
13. Lischke, S.; Knoll, D.; Mai, C.; Zimmermann, L.; Peczek, A.; Kroh, M.; Trusch, A.; Krune, E.; Voigt, K.; Mai, A. High bandwidth, high responsivity waveguide-coupled germanium p-i-n photodiode. *Opt. Express* **2015**, *23*, 27213–27220. [CrossRef] [PubMed]
14. Chen, H.; Verheyen, P.; de Heyn, P.; Lepage, G.; de Coster, J.; Balakrishnan, S.; Absil, P.; Yao, W.; Shen, L.; Roelkens, G.; et al. −1 V bias 67 GHz bandwidth Si-contacted germanium waveguide p-i-n photodetector for optical links at 56 Gbps and beyond. *Opt. Express* **2016**, *24*, 4622–4631. [CrossRef] [PubMed]
15. Frova, A.; Handler, P. Franz-Keldysh effect in the space-charge region of a germanium p-n junction. *Phys. Rev.* **1965**, *137*, A1857. [CrossRef]
16. Sun, C.; Wade, M.T.; Lee, Y.; Orcutt, J.S.; Alloatti, L.; Georgas, M.S.; Waterman, A.S.; Shainline, J.M.; Avizienis, R.R.; Lin, S.; et al. Single-chip microprocessor that communicates directly using light. *Nature* **2015**, *528*, 534–538. [CrossRef] [PubMed]
17. Chaisakul, P.; Marris-Morini, D.; Frigerio, J.; Chrastina, D.; Rouifed, M.-S.; Cecchi, S.; Crozat, P.; Isella, G.; Vivien, L. Integrated germanium optical interconnects on silicon substrates. *Nat. Photonics* **2014**, *8*, 482–488. [CrossRef]
18. Goll, B.; Thomson, D.J.; Zimmermann, L.; Porte, H.; Gardes, F.Y.; Hu, Y.; Knoll, D.; Lischke, S.; Tillack, B.; Reed, G.T.; et al. A monolithically integrated silicon modulator with a 10 Gb/s 5 Vpp or 5.6 Vpp driver in 0.25 μm SiGe:C BiCMOS. *Front. Phys.* **2014**, *2*, 62. [CrossRef]
19. Shang, K.; Pathak, S.; Guan, B.; Liu, G.; Yoo, S.J.B. Low-loss compact multilayer silicon nitride platform for 3D photonic integrated circuits. *Opt. Express* **2015**, *23*, 21334–21342. [CrossRef]
20. Rahim, A.; Ryckeboer, E.; Subramanian, A.Z.; Clemmen, S.; Kuyken, B.; Dhakal, A.; Raza, A.; Hermans, A.; Muneeb, M.; Dhoore, S.; et al. Expanding the silicon photonics portfolio with silicon nitride photonic integrated circuits. *J. Lightwave Technol.* **2017**, *35*, 639–649. [CrossRef]
21. Wilmart, Q.; el Dirani, H.; Tyler, N.; Fowler, D.; Malhouitre, S.; Garcia, S.; Casale, M.; Kerdiles, S.; Hassan, K.; Monat, C.; et al. A versatile silicon-silicon nitride photonics platform for enhanced functionalities and applications. *Appl. Sci.* **2019**, *9*, 255. [CrossRef]
22. Muñoz, P.; Micó, G.; Bru, L.A.; Pastor, D.; Pérez, D.; Doménech, J.D.; Fernández, J.; Baños, R.; Gargallo, B.; Alemany, R.; et al. Silicon nitride photonic integration platforms for visible, near-infrared and mid-infrared applications. *Sensors* **2017**, *17*, 2088. [CrossRef] [PubMed]
23. Zhang, Z.; Yako, M.; Ju, K.; Kawai, N.; Chaisakul, P.; Tsuchizawa, T.; Hikita, M.; Yamada, K.; Ishikawa, Y.; Wada, K. A new material platform of Si photonics for implementing architecture of dense wavelength division multiplexing on Si bulk wafer. *Sci. Technol. Adv. Mater.* **2017**, *18*, 283–293. [CrossRef] [PubMed]
24. Chen, L.; Doerr, C.R.; Buhl, L.; Baeyens, Y.; Aroca, R.A. Monolithically integrated 40-wavelength demultiplexer and photodetector array on silicon. *IEEE Photonics Technol. Lett.* **2011**, *23*, 869–871. [CrossRef]
25. Chen, L.; Doerr, C.R.; Dong, P.; Chen, Y.-K. Monolithic silicon chip with 10 modulator channels at 25 Gbps and 100-GHz spacing. *Opt. Express* **2011**, *19*, B946–B951. [CrossRef] [PubMed]
26. Mao, S.C.; Tao, S.H.; Xu, Y.L.; Sun, X.W.; Yu, M.B.; Lo, G.Q.; Kwong, D.L. Low propagation loss SiN optical waveguide prepared by optimal low-hydrogen module. *Opt. Express* **2008**, *16*, 20809–20816. [CrossRef] [PubMed]
27. Rangarajan, B.; Kovalgin, A.Y.; Wörhoff, K.; Schmitz, J. Low-temperature deposition of high-quality silicon oxynitride films for CMOS-integrated optics. *Opt. Lett.* **2013**, *38*, 941–943. [CrossRef] [PubMed]
28. Liu, J.; Pan, D.; Jongthammanurak, S.; Wada, K.; Kimerling, L.C.; Michel, J. Design of monolithically integrated GeSi electroabsorption modulators and photodetectors on an SOI platform. *Opt. Express* **2007**, *15*, 623–628. [CrossRef]
29. Nguyen, L.M.; Kuroyanagi, R.; Tsuchizawa, T.; Ishikawa, Y.; Yamada, K.; Wada, K. Stress tuning of the fundamental absorption edge of pure germanium waveguides. *Opt. Express* **2015**, *23*, 18487–18492. [CrossRef]
30. Ahn, D.; Hong, C.-Y.; Liu, J.; Giziewicz, W.; Beals, M.; Kimerling, L.C.; Michel, J.; Chen, J.; Kärtner, F.X. High performance, waveguide integrated Ge photodetectors. *Opt. Express* **2007**, *15*, 3916–3921. [CrossRef]
31. Ahna, D.; Kimerling, L.C.; Michel, J. Efficient evanescent wave coupling conditions for waveguide-integrated thin-film Si/Ge photodetectors on silicon-on-insulator/germanium-on-insulator substrates. *J. Appl. Phys.* **2011**, *110*, 083115. [CrossRef]

32. Chaisakul, P.; Koompai, N.; Limsuwan, P. Theoretical investigation of a low-voltage Ge/SiGe multiple quantum wells optical modulator operating at 1310 nm integrated with Si3N4 waveguides. *AIP Adv.* **2018**, *8*, 115318. [CrossRef]
33. Chaisakul, P.; Vakarin, V.; Frigerio, J.; Chrastina, D.; Isella, G.; Vivien, L.; Marris-Morini, D. Recent progress on Ge/SiGe quantum well optical modulators, detectors, and emitters for optical interconnects. *Photonics* **2019**, *6*, 24. [CrossRef]
34. Hernández-Montero, W.W.; Zaldívar-Huerta, I.E.; Zúñiga-Islas, C.; Torres-Jácome, A.; Reyes-Betanzo, C.; Itzmoyotl-Toxqui, A. Optical and compositional properties of amorphous silicon-germanium films by plasma processing for integrated photonics. *Opt. Mater. Express* **2012**, *2*, 358–370. [CrossRef]
35. Selvaraja, S.; de Heyn, P.; Winroth, G.; Ong, P.; Lepage, G.; Cailler, C.; Rigny, A.; Bourdelle, K.; Bogaerts, W.; van Thourhout, D.; et al. Highly uniform and low-loss passive silicon photonics devices using a 300 mm CMOS platform. In Proceedings of the Optical Fiber Communication Conference (OFC2014), San Francisco, CA, USA, 9–13 March 2014; p. Th2A.33.
36. Abdolvand, R.; Ayazi, F. An advanced reactive ion etching process for very high aspect-ratio sub-micron wide trenches in silicon. *Sens. Actuators A Phys.* **2008**, *144*, 109–116. [CrossRef]
37. Wu, B.; Kumar, A.; Pamarthy, S. High aspect ratio silicon etch: A review. *J. Appl. Phys.* **2010**, *108*, 051101. [CrossRef]